

Exploring natural genetic diversity in a bread wheat multi-founder population: Dual imaging of photosynthesis and stomatal kinetics.

Michele Faralli[#], Greg Mellers¹, Shellie Wall, Silvere Vialet-Chabrand[†], Guillaume Forget³, Alexander Galle², Jeron Van Rie², Keith A. Gardner¹⁺, Eric S. Ober¹, James Cockram¹, Tracy Lawson^{*}

School of Life Sciences, University of Essex, Colchester CO4 3SQ, UK

¹ NIAB, 93 Lawrence Weaver Road, Cambridge CB3 0LE, UK

² BASF Belgium Coordination Center CommV-Innovation Center Gent, Technologiepark-Zwijnaarde 101, 9052 Gent, Belgium

³ University of Bordeaux, INRAE, UMR BIOGECO, Pessac 33615, France

[#] Present address: Centre Agriculture Food Environment (C3A), University of Trento, Via Mach 1, San Michele all'Adige, 38010 Trento, Italy

[†] Present address: Horticulture and Product Physiology; WUR; Droevendaalsesteeg 1, 6708PB, Wageningen, The Netherlands

⁺ International Maize and Wheat Improvement Center (CIMMYT), Carretera México-Veracruz, Mexico

^{*} Corresponding Author: tlawson@essex.ac.uk

One-sentence summary: Significant variation exists in stomatal dynamics and photosynthetic capacity in a magic bread wheat population.

© The Author(s) 2024. Published by Oxford University Press on behalf of the Society for Experimental Biology.

This is an Open Access article distributed under the terms of the Creative Commons Attribution License (<https://creativecommons.org/licenses/by/4.0/>), which permits unrestricted reuse, distribution, and reproduction in any medium, provided the original work is properly cited.

Abstract

A better understanding of crop phenotype under dynamic environmental conditions will help inform the development of new cultivars with superior adaptation to constantly changing field conditions. Recent research has shown that optimising photosynthetic and stomatal conductance traits holds promise for improved crop performance. However, standard phenotyping tools such as gas-exchange systems are limited by their throughput. In this work, a novel approach based on a bespoke gas-exchange chamber allowing combined measurement of the quantum yield of photosystem II (PSII) with an estimation of stomatal conductance via thermal imaging, was used to phenotype a range of bread wheat (*Triticum aestivum* L.) genotypes, that were a sub-set of a multi-founder experimental population. Datasets were further supplemented by measurement of photosynthetic capacity and stomatal density. First, we showed that measurement of stomatal traits using our dual imaging system compared to standard IRGA methods showed good agreement between the two methods ($R^2=0.86$) for the rapidity of stomatal opening (K_i), with the dual-imager method resulting in less intra-genotype variation. Using the dual-imaging methods, and traditional approaches we found broad and significant variation in key traits, including photosynthetic CO_2 uptake at saturating light and ambient CO_2 concentration (A_{sat}), photosynthetic CO_2 uptake at saturating light and elevated CO_2 concentration (A_{max}), the maximum velocity of Rubisco for carboxylation (V_{cmax}), time for stomatal opening (K_i), and leaf evaporative cooling. Anatomical analysis revealed significant variation in flag leaf adaxial stomatal density. Associations between traits highlighted significant relationships between leaf evaporative cooling, leaf stomatal conductance under low (g_{smin}) and high (g_{smax}) light intensity, and the operating efficiency of PSII (F_q'/F_m), highlighting the importance of stomatal conductance and stomatal rapidity in maintaining optimal leaf temperature for photosynthesis in wheat. Additionally, g_{smin} and g_{smax} were positively associated, indicating that potential combination of preferable traits (i.e. inherently high g_{smax} , low K_i and maintained leaf evaporative cooling) are present in wheat. This work highlights for the first time the effectiveness of thermal imaging in screening dynamic stomatal conductance in a large panel of wheat genotypes. The wide phenotypic variation observed suggested the presence of exploitable genetic variability in bread wheat for dynamic stomatal conductance traits and photosynthetic capacity for targeted optimisation within future breeding programs.

Key words: MAGIC, photosynthetic capacity, photosynthesis, Wheat, stomatal conductance, water use efficiency, kinetics, thermal images.

Introduction

Crop yield is the product of the cumulative rates of photosynthesis over the growing season (Zelitch, 1982). Indeed, several developmental processes occurring throughout the life cycle of a crop co-determine a series of yield components that are often limited by the availability of assimilates (Slafer, 2003). For instance, free-air concentration enrichment experiments (Long *et al.*, 2006) and bioengineering approaches (Driever *et al.*, 2017) have provided evidence that increasing rates of photosynthesis can lead to yield gains. In many crops, while harvest index and light interception capacity are approaching their theoretical maximum (~0.64 and 0.8–0.9 respectively, Long *et al.*, 2006), the efficiency of energy conversion into biomass (i.e., radiation-use efficiency and thus photosynthesis) still has substantial room for improvement (Long *et al.*, 2006). Although it is well established that significant variation in photosynthesis exists between species (e.g. Wullschleger *et al.*, 1993; Lawson *et al.*, 2012) several more recent studies have reported significant variation between cultivars of the same species (Driever, *et al.*, 2014; Carmo-Silva *et al.*, 2017; Faralli *et al.*, 2019; 2020; McAusland *et al.*, 2020; Ferguson *et al.* 2020; Wall *et al.*, 2023). Most of the intraspecific natural variation in photosynthesis for C₃ plants has been attributed to differences in biochemical capacity, including electron transport rates and carboxylation efficiency (Driever *et al.*, 2014; Carmo-Silva *et al.*, 2017). In addition, under natural dynamic conditions photosynthetic processes such as activation of Calvin cycle enzymes and/or stomatal dynamics can also be limiting (Lawson and Blatt, 2014; Taylor and Long, 2017; Salter *et al.*, 2019; Faralli *et al.* 2019).

Stomatal dynamics balance leaf CO₂ uptake and water loss and hence significantly influence the key components of crop productivity: the cumulative rate of photosynthesis; water use and evaporative cooling. The opening and closing of stomata are driven by a series of environmental, hormonal and hydraulic signals (Blatt, 2000) with significant variation observed in sensitivity and responsiveness among different species (Lawson *et al.*, 1998; Lawson *et al.*, 2003, Lawson *et al.*, 2012; Lawson, 2009) and genotypes driven by differences in morphology (Weyers & Lawson, 1997; Weyers *et al.*, 1997; Hetherington and Woodward, 2003; Drake *et al.*, 2013; McAusland *et al.*, 2015; Yoshiyama *et al.*, 2024). In general, stomata open in response to increasing light intensity, low CO₂ concentration ([CO₂]), high temperatures, and low vapor pressure deficit (VPD), while closure is driven by low light or darkness, high [CO₂], and high VPD (Outlaw, 2003). In the natural environment, these factors can occur simultaneously and in a dynamic and fluctuating manner (Sharkey and Raschke, 1981; Zeiger and Zhu 1998; Talbott *et al.*, 2003;).

It has been extensively shown that the rapidity in stomatal movements under conditions such as shade or sun-flecks may be considered preferable traits for crop improvement due to reduced water when carbon gain is limited and a reducing diffusional constraint on photosynthesis (Lawson *et al.*, 2010; Lawson & Blatt, 2014). In wheat (*Triticum aestivum* L.), a major food crop accounting for up to 20% of the world's calorie consumption (Erenstein *et al.* 2022), these traits have been sparsely explored (Faralli *et al.* 2019), although in other crops (e.g. rice) stomatal rapidity has been associated with an adaptation to dry conditions (Qu *et al.* 2016; Zhang *et al.* 2019; Faralli *et al.* 2019). Therefore, the main objective of this work was to phenotype, via a novel, non-invasive and high throughput method, stomatal rapidity in a wheat multi-parent advanced generation inter-cross (MAGIC) population along with steady-state gas-exchange traits. A total of 192 greenhouse-grown wheat genotypes were analysed, including photosynthetic capacity and stomatal traits. Our work is the largest phenotyping study carried out so far to characterize wheat stomatal response and photosynthetic diversity under dynamic light response and may provide methods and resources to open up new avenues to optimize wheat responses to natural fluctuating environmental conditions.

Materials and methods

Plant material

The MAGIC wheat population was used in this study (Mackay *et al.* 2014). The population consists of recombinant inbred lines (RILs) generated from three cycles of intercrossing between eight elite European wheat cultivars (Alchemy, Brompton, Claire, Hereward, Rialto, Robigus, Soissons, Xi-19) followed by five rounds of self-pollination to derive RILs as described by Mackay *et al.* (2014). A subset of the population comprising of 192 lines and the eight parental lines was used for this work. These lines encompassed the important genetic variation present in the larger population.

Plant growth, vernalization and experimental design

Seeds were sown in plastic trays containing compost and germinated in a growth cabinet (Reftech BV, Sassenheim, the Netherlands) at the University of Essex at $\sim 200 \mu\text{mol m}^{-2} \text{s}^{-1}$ photosynthetic photon flux density (PPFD), 14h/10h photoperiod (light/dark), $\sim 15^\circ\text{C}$ on average and $\sim 60\%$ relative humidity (RH). The compost (Levington F2S; Everris, Ipswich, UK) contained coir, sand and fertiliser ($144 \text{ mg L}^{-1} \text{ N}$, $73 \text{ mg L}^{-1} \text{ P}$, $239 \text{ mg L}^{-1} \text{ K}$, adjusted to pH 5.3-6.0 with dolomitic lime). At BBCH (Biologische Bundesanstalt, Bundessortenamt und Chemische Industrie) growth stage (GS) 12 (GS12, two seedling leaves unfolded; Lancashire *et al.*, 1991) seedlings were moved into a cold room for vernalization: 4°C , ~ 50

$\mu\text{mol m}^{-2} \text{ s}^{-1}$ PPFD at 10h/14h photoperiod (light/dark) for eight weeks. After vernalization, seedlings (one per pot) were transplanted into 1.5 L pots (15 cm diameter; 12 cm deep) containing F2S compost and transferred to a temperature-controlled glasshouse. To phenotype the population at flag leaf emergence (GS 39-41), three batches of plants were grown from July 2017 to April 2018. Batch 1 consisted of 189 genotypes, with each line replicated twice. In Batch 2, 186 of these genotypes were grown again ($n=2$), but the eight parental lines had a higher number of replication ($n=5$). Batch 3 included an extra replicate of contrasting lines from Batch 1 (48 genotypes) and Batch 2 (47 genotypes) as well as 80 extra genotypes in $n=2$, along with eight-fold ($n=8$) parental replication. After vernalization, plants from each batch were transferred to the glasshouse and spatially randomized with a two-block structure and genotypes exhibiting a non-uniform behaviour between replicates were discarded from the study (see supplementary Figure 1).

Phenotypic analysis

Plants were scored for the occurrence of flag leaf emergence (growth stage [GS] 39) and GS 41 (flag leaf fully emerged). Plant height (soil surface to flag leaf tip) at GS 41 was assessed with a ruler prior to stomatal conductance analysis. All measurements were made on flag leaves of plants that had reached GS41-45.

High throughput phenotyping of dynamic g_s responses with thermal imaging

Thermal imaging

Dynamic responses of stomatal conductance to water vapour (g_s) to a step-change in irradiance were assessed by modifying an in-house system developed at University of Essex (McAusland et al., 2013). A FluorImager system (Technologica, Colchester, Essex, UK) was modified to allow thermal imaging and chlorophyll fluorescence imaging simultaneously. For thermal imaging, a thermal camera Optris 450i (Optris GmbH, Berlin, DE) with a temperature resolution of 0.1 °C, was configured with an emissivity (ϵ) of 0.96 and set to perform a non-uniform calibration every minute. The thermal camera was positioned at 0.45 m in the original location of the chlorophyll fluorescence camera, directly above the imaging port while the chlorophyll fluorescence camera AVT manta (Allied Vision, Stadtroda, DE) was positioned at a 90° angle. A silver-coated mirror (Thor-Optics, Dachau, Germany) was hinged on an axis directly above the original camera port and a servo motor connected to an Arduino was used to automatically move the mirror switching between the two cameras while keeping the same field of view (see Supplementary Figure 1). Air temperature and relative humidity were collected using a sensor (HygroClip2, HC2A-S, Rotronic, Bassersdorf, CH) connected to the same Arduino. A custom software was used to automatically collect

images from both cameras, record environmental data, operate the servo motor and process the data.

Imaging chamber and gas control

A modified open-top chamber based on that described McAusland *et al.* (2013) was designed and constructed. The cuvette allowed the control of gases concentration (N₂, H₂O, CO₂, and O₂), while keeping an open top for imaging. The chamber was built from Perspex and due to the relatively high reflection inside the chamber at high light intensity, the interior surfaces were painted grey. With the exception of the base, the chamber consisted of an inner and outer wall separated by a 10mm gap. The outer walls were connected on each of the four sides by 6 mm PTFE tubing connections that fed gas into the chamber wall cavity. The inner wall was perforated with 1 mm diameter holes at a density of 9 per 100mm², which was optimal for maintaining homogenous gas concentrations whilst minimizing leaf movement through turbulence. Within the chamber, target gas concentrations of nitrogen (N₂), and CO₂ were individually maintained by mass flow controllers (EL Flow, Bronkhorst, Ruurlo, The Netherlands), connected to compressed gas cylinders containing 100% N₂, and CO₂, respectively (British Oxygen Company-Industrial Gases, Ipswich, UK). To control water vapour concentration, a Controlled Evaporation and Mixing system (CEM Evaporator W-202A, Bronkhorst, Newmarket, UK) was used to precisely regulate the water vapour content of the air. Gas composition in the chamber was monitored at leaf height by sampling air with a diaphragm pump (Type 124, ADC Hoddesdon, Herts, UK) at 500 cm³ min⁻¹. Both CO₂ and H₂O vapour concentrations were measured with an infrared gas analyser (IRGA) (Li-840, LI-COR, NE, USA). Throughout the phenotyping experiment and during each analysis, ambient CO₂ concentration (C_a) was maintained at 400 μmol CO₂ mol⁻¹ air while relative humidity (RH) was maintained at 45-60% inside the cuvette.

Estimating dynamic stomatal conductance from leaf temperature

Significant negative correlation exists between leaf conductance to water vapour and leaf temperature (Jones, 2009). Due to the transition of water into water vapour during transpiration, energy (latent heat of vaporization) is taken from the leaf, leading to a reduction in surface leaf temperature. This evaporative cooling effect of transpiration can be used as an indirect method for the estimation for leaf stomatal conductance (g_s) (Supplementary Figure 1). For this reason, g_s was estimated following the equations proposed by Leinonen *et al.* (2006) and shown in Jones *et al.* (2009).

Mass leaf transpiration was estimated as follows:

$$E_m = \frac{[0.92g_b + \left(\frac{4\epsilon\sigma T_a^3}{\rho C_p}\right)](\rho C_p)(T_{dry} - T_{leaf})}{\lambda}$$

Where g_b is the estimated boundary layer conductance to water vapour (see Supplementary Dataset S1 for an example of calculation), 0.92 indicates a proportional relationship between heat and water vapour transfer rates across the boundary layer under laminar flow, ϵ represents sample emissivity, σ the Stefan-Boltzmann constant, T_a is air temperature, ρ represent air density, C_p the air specific heat capacity, T_{dry} is the temperature of the dry reference and T_{leaf} is the temperature of the leaf sample and λ is the latent heat of vaporization.

Conversion of E_m to $\text{mol m}^{-2} \text{s}^{-1}$ was carried out and total conductance to water vapour was estimated as:

$$g_w = \frac{E}{\frac{e_s - e_a}{P}}$$

where E is leaf transpiration, e_s is the saturated water vapour pressure in the leaf, e_a is the air vapour pressure and P is the atmospheric pressure (i.e. leaf vapour pressure deficit, VPD).

Leaf stomatal conductance to water vapour (g_s) was then estimated as

$$g_s = \frac{1}{\frac{1}{g_w} - \frac{1}{g_b}}$$

A spreadsheet containing an example of calculating g_s from thermography and environmental conditions is provided in Supplementary Dataset S2.

Protocol for estimating parameters in response to step changes in irradiance

Prior to each analysis plants were moved from the greenhouse to a controlled environment dark room (20°C maintained with an air conditioner and ~60% RH maintained with a humidifier). It was possible to run three plants simultaneously and the dry reference. The dry reference was a flag leaf sampled with scissors from spare plants for each protocol and petroleum jelly (Vaseline) was applied on both surfaces to prevent transpiration. Dark adapted plants (~1h per cycle, please see below) were clamped onto the chamber and acclimated for 16 minutes at $100 \mu\text{mol m}^{-2} \text{s}^{-1}$ photosynthetic photon flu density (PPFD) followed by a step-change in light to $1000 \mu\text{mol m}^{-2} \text{s}^{-1}$ PPFD for 30 minutes (sufficient to reach steady state in wheat, Faralli *et al.* 2019) and thermal and fluorescence images were

taken every 2 minutes. The thermal dataset generated was automatically analysed with a bespoke system based on OpenCV that estimates leaf g_s in a pixel-based manner and averages over the leaf sample. Leaf segmentation was carried out using basal fluorescence in the dark and by applying Otsu thresholding. The time constant for the rapidity of g_s response to a step change in light intensity (K_{gs} – estimated from g_s kinetics, or K_t – estimated from $T_{dry}-T_{leaf}$ kinetics) was estimated with the model proposed by Vialet-Chabrand (2013). The dynamic model predicts the temporal response of g_s at the leaf level using a sigmoid function for increasing g_s . It describes the temporal response of g_s using a time constant (k , min), an initial time lag (λ , min) and a steady-state g_s reached at given PPFD. The model allowed also the estimation of g_s at 100 $\mu\text{mol m}^{-2} \text{s}^{-1}$ PPFD (g_{smin}) and g_s at 1000 $\mu\text{mol m}^{-2} \text{s}^{-1}$ PPFD (g_{smax}). In addition, ΔT was estimated as the difference in temperature also allowed the first point after the step-change in light and the last point (i.e. cooling capacity). Light-adapted quantum yield of photosystem II (F_q/F_m) at low and high light were also assessed as well as non-photochemical quenching (high light) were also estimated from fluorescence camera following Murchie and Lawson (2013).

Photosynthetic CO₂ response curves (A/C_i)

The same leaf used for imaging was subjected to gas exchange measurements. Photosynthesis measurements (A/C_i curves) were performed between 9:00 and 15:00 on the fully emerged flag leaf at GS41-45 using a LI-6400. Measurements of the response of A to sub-stomatal CO₂ concentrations (C_i) were performed in the middle of the tagged leaf using an open infrared gas exchange system and a 2 cm² leaf cuvette with an integral blue–red LED light source (LI-6400–40; LI-COR, Lincoln, NE, United States). In the cuvette, PPFD was maintained at a saturating level of 1500 $\mu\text{mol m}^{-2} \text{s}^{-1}$, a leaf temperature of $20 \pm 0.1^\circ\text{C}$, a VPD between 0.9 and 1.3 kPa and a Ca of 400 $\mu\text{mol mol}^{-1}$. When steady-state conditions were achieved, Ca was sequentially decreased to 300, 200, 100 and 75 $\mu\text{mol mol}^{-1}$ before returning to the initial concentration of 400 $\mu\text{mol mol}^{-1}$. This was followed by a sequential increase to 550, 700, 1000, and 1200 $\mu\text{mol mol}^{-1}$. Readings were recorded when A had stabilized to the new conditions. The maximum velocity of Rubisco for carboxylation ($V_{C_{max}}$) and the maximum rate of electron transport demand for Ribulose 1,5-bisphosphate (RuBP) regeneration (J_{max}) were derived by curve fitting. We used the *Plantecophys* R package to determine $V_{C_{max}}$, J_{max} via non-linear least squares while standard errors of the parameters were estimated with standard methods (Supplementary Figure 1).

Validation of estimate g_s dataset with thermal imaging

An additional experiment was conducted to validate image-based estimations of g_s by comparison with g_s values estimated using standard gas-exchange measurements. Lines with contrasting K_{gs} values were grown as for the phenotyping experiment. IRGAs (Li-Cor 6400XT) assessed the rapidity of stomatal responses to a step-change in light (using the same protocols as described by Faralli *et al.*, (2019)). Briefly, prior to measurement, flag leaves of plants at GS41 were equilibrated to a PPFD of $100 \mu\text{mol m}^{-2} \text{s}^{-1}$ for approximately 60 min or until g_s reached 'steady state', defined as a $\leq 2\%$ change in rate during a 10 min period. After equilibration PPFD was increased to $1500 \mu\text{mol m}^{-2} \text{s}^{-1}$ for 50 min and subsequently returned to $100 \mu\text{mol m}^{-2} \text{s}^{-1}$ for 1h. Conditions inside the leaf cuvette were kept constant at $20^\circ\text{C} \pm 0.1$ leaf temperature, a VPD of 1kPa with a dew point generator (LI-610; LI-COR, Lincoln, NE), and $400 \mu\text{mol CO}_2 \text{ mol}^{-1}$ air (ambient CO_2 concentration, C_a). The time constant for the rapidity of g_s responses to a step change in light intensity was estimated as previously described.

Statistical analysis

Data analysis was conducted using Rstudio. Due to significant variation in growing conditions in the glass house and spatial effects the data were analysed using a one-way analysis of covariance (ANCOVA), treating 'greenhouse' and 'block' as covariates. Normality checks were performed on all data sets. The associations between different traits were examined through correlation analysis, and the Pearson test was used to evaluate the strength of these associations.

Results

Comparison of g_s values obtained from imaging and standard approaches.

To evaluate g_s values obtained from the dual imaging system with those from standard IRGA methods, a comparative analysis was performed on a sub-set of genotypes, selected based on their differential kinetic profiles (Fig.1). Overall, the time constant for stomatal opening (K_i) as determined by the dual-imager method and standard gas-exchange showed no significant difference between the two methods (Fig. 1A) ($p > 0.05$). Additionally, a positive and significant association was observed for dual imager and infra-red gas analyser estimates of K_i (Fig. 1B). Generally, the dual imager method showed higher variation between genotypes compared to the infra-red gas analyser, yet the ranking among lines remained consistent.

Photosynthetic capacity

The response of photosynthetic assimilation rate to increasing CO₂ at saturating irradiance (A/C_i response curve) was analysed for all lines to assess variation in photosynthetic capacity. A/C_i curves for all genotypes measured followed the typical hyperbolic response (data not shown). From these response curves, both the light saturated rate of photosynthesis (A_{sat}) and the light and CO₂ saturated rate of photosynthesis (A_{max}) were determined. Significant differences ($p < 0.05$, Fig. 2) were observed between genotypes in both values, indicating variation in the maximum photosynthetic potential as well as operational rate across these genotypes. A_{sat} varied from a minimum of 18 to a maximum of 34 $\mu\text{mol m}^{-2} \text{s}^{-1}$ on average. For the eight parental lines, 'Hereward' and 'Robigus' showed the lowest (20-21.5 $\mu\text{mol m}^{-2} \text{s}^{-1}$) values, while the highest values (27-28 $\mu\text{mol m}^{-2} \text{s}^{-1}$) were observed in 'Soissons', 'Claire' and 'Xi19'. For recombinant inbred lines of the population, the highest values were observed for MEL_122_1b and MEL_036_8 (up to 34 $\mu\text{mol m}^{-2} \text{s}^{-1}$) while the lowest values between 15 and 18 $\mu\text{mol m}^{-2} \text{s}^{-1}$ were observed in MEL_139_7 and MEL_071_1c. A_{max} varied significantly between genotypes with values ranging from 25 to 45 $\mu\text{mol m}^{-2} \text{s}^{-1}$ on average, and a positive association between A_{sat} and A_{max} was observed ($p < 0.001$). However, in some cases, the ranking was significantly altered, e.g. Robigus had a relatively low A_{sat} while it was positioned in the middle of the distribution for A_{max} . A_{sat} and A_{max} for the 200 lines measured followed a normal distribution. Therefore, the differential ranking of lines between operational assimilation rates (A_{sat}) and maximum capacity (A_{max}) clearly indicates that these are influenced by differing factors and that a high photosynthetic potential does not always translate to a higher actual rate in the field.

Significant variation in V_{cmax} was observed between genotypes ($p < 0.05$, Fig. 3) with values varying >3 fold (from 90 $\mu\text{mol m}^{-2} \text{s}^{-1}$ to 270 $\mu\text{mol m}^{-2} \text{s}^{-1}$). As stated above, on average for parental lines, 'Hereward' showed the lowest (140 $\mu\text{mol m}^{-2} \text{s}^{-1}$) values along with 'Robigus' (135 $\mu\text{mol m}^{-2} \text{s}^{-1}$) while higher values were observed for 'Xi19' and 'Soissons' (180 $\mu\text{mol m}^{-2} \text{s}^{-1}$). For recombinant inbred lines, MEL_139_7 and MEL_073_8 had the lowest values (around 90 $\mu\text{mol m}^{-2} \text{s}^{-1}$) while the highest values were observed for MEL_062_1a and MEL_170_3 (280-300 $\mu\text{mol m}^{-2} \text{s}^{-1}$). The maximum electron transport rate capacity for RuBP regeneration (J_{max}) also showed variation (although borderline significant, $p = 0.059$) between genotypes and ranged from between 100 and 310 $\mu\text{mol m}^{-2} \text{s}^{-1}$ on average.

In the field, the realised assimilation rate is influenced by g_s and the potential imposed diffusional constraints due to the dynamic behaviour of stomata. In order to assess stomatal dynamics in all 200 lines, a dual imager was utilized that adopted a high-resolution thermal

camera to assess changes in leaf temperature as a proxy of g_s response (McAusland et al., 2013; Vialet-Chabrand & Lawson, 2019; 2020) to a step increase in light intensity. Stomatal conductance values following 30 min at sub-saturating light intensity ($1000 \mu\text{mol m}^{-2} \text{s}^{-1}$) ($g_{s\text{max}}$) showed trends of variation ($p=0.064$) between lines, and an average value of $0.7 \text{ mol m}^{-2} \text{s}^{-1}$ (Figure 4A). However, unsurprisingly, significant variation in individual measurements within the replicates was high (average SEM $0.1 \text{ mol m}^{-2} \text{s}^{-1}$). In the parental lines, the lowest $g_{s\text{max}}$ values ($0.6 \text{ mol m}^{-2} \text{s}^{-1}$) were observed in Robigus while Rialto displayed the highest value ($0.85 \text{ mol m}^{-2} \text{s}^{-1}$). Several recombinant inbred lines had low $g_{s\text{max}}$ ranking from 0.3 to $0.5 \text{ mol m}^{-2} \text{s}^{-1}$ (e.g. MEL_078_1cA and MEL_179_2). The rapidity of changes in g_s after a 30 min sun-flecks, measured as the time constant to reach 63% of $g_{s\text{max}}$ (K_i) varied greatly between lines ($p<0.001$) and values ranged between 1.9 to 19 minutes (Figure 4B). For the parental material, Rialto, Brompton and Hereward had the fastest responses (5 to 8 minutes on average) while Xi19 and Alchemy showed the slowest (10 min). MEL_146_1b and MEL_203_3 had a very quick stomatal responses (K_i between 1.9 and 2.5 minutes) while MEL_102_1 and MEL_071_1c had the slowest stomatal response (16 minutes). K_i values followed a normal distribution with the majority of speeds of responses between 5 and 13 min which agrees with previous reports on wheat (Faralli *et al.*, 2019) (see Supplementary Figure 4). Changes in stomatal conductance with differences in light intensity are critically important for evaporative cooling and maintaining optimal leaf temperature for photosynthesis and other metabolic processes. Differences between leaf temperature driven by the 30 min sun-fleck (i.e. cooling capacity, δT) showed significant and wide variation with lines and illustrates the ability of these lines to counteract the increase in irradiance via transpiration (i.e. positive evaporative cooling) (Figure 4C). Values for δT ranged between -2 to $4 \text{ }^\circ\text{C}$ changes in leaf temperatures. Values below zero indicate limited evaporative cooling with higher light intensity whilst positive values show that changes in g_s result in increased cooling capacity. Most of the population (70%) showed positive values (i.e. cooling capacity) and all the parental material showed positive values with Xi19, Robigus and Alchemy showing the highest values (δT 1.5°C on average). For the parental lines, the lowest values were observed for Hereward and Rialto (δT $0.5 \text{ }^\circ\text{C}$) while MEL_081_3 and MEL_191_2 had the most negative values (δT $-2 \text{ }^\circ\text{C}$). Significant differences were also observed for δg_s i.e. the change in stomatal conductance after a step-change in light (Figure 4D). In general, δg_s ranked from 0.2 to up to $0.9 \text{ mol m}^{-2} \text{s}^{-1}$ with Alchemy showing the highest values between parental lines ($0.7 \text{ mol m}^{-2} \text{s}^{-1}$) while Brompton and Rialto the lowest ($0.5 \text{ mol m}^{-2} \text{s}^{-1}$). MEL_201_5 and MEL_006_1 showed the highest delta between $g_{s\text{min}}$ and $g_{s\text{max}}$ ($0.9 \text{ mol m}^{-2} \text{s}^{-1}$) while MEL_005_3 and MEL_036_1b the lowest ($0.2 \text{ mol m}^{-2} \text{s}^{-1}$).

The operating efficiency of PSII (Fq'/Fm') at low light levels showed significant variation between lines ($p=0.048$) with an average value of 0.62 (Figure 5A). In the parental lines, the lowest operating efficiency was observed in Soissons while Rialto displayed the highest value (0.68). When plants were exposed to the sub-saturating light intensity of $1000 \mu\text{mol m}^{-2} \text{s}^{-1}$, operating efficiency decreased and no significant differences were observed between lines. Similarly, although variation was present for NPQ, however this was not significantly different between lines, potentially due to the sub-saturating light conditions at which the plants were exposed.

Stomatal density

Adaxial stomatal density was generally greater than abaxial density in all lines, which is typical for wheat although uncommon in most other species (Wall *et al.* 2022). Adaxial stomatal density showed significant ($p<0.05$, Figure 6A) variation between lines analysed, with average SD values ranging between 50 to 80 stomata mm^{-2} , while average abaxial SD values were between 40 and 65 stomata mm^{-2} . Alchemy and Soissons had the highest average SDs (57 and 61 stomata mm^{-2} respectively) of the parental lines while Claire had the lowest (50 stomata mm^{-2}). There was a strong positive correlation ($p<0.001$) between adaxial and abaxial stomatal density (Fig. 8), suggesting a link between the two surfaces in terms of cell differentiation into guard cells.

Correlation analysis including all measurements parameters showed a number of significant associations (Fig. 7). Significant correlations ($p<0.05$) were observed between A_{sat} , A_{max} , V_{cmax} and J_{max} . No significant associations were observed between stomatal anatomical features and estimated dynamic or steady state g_s traits. However, a negative and significant correlation was observed between g_{smin} and K_i ($p<0.001$). Similarly, δT significantly and positively correlated with K_i while a negative association existed between δT and g_{smin} . δg_s was correlated with several traits (J_{max} and A_{max}) and, in particular, with δT ($r=0.47$).

Discussion

The need to double food production in the next 50 years to feed a growing human population (Ray et al., 2019; Asseng et al., 2020; Furbank et al., 2020; Billen et al., 2024) and the requirement to do so in the face of predicted climate changes has led to increased research efforts to improve photosynthesis and other physiological processes in crops. Genetic modification (GM) of photosynthetic pathways has already proven successful (Raines, 2011; Evans, 2013; Voss-Fels et al., 2019; Kromdijk et al., 2016; South et al., 2019), however, GM production is still met with resistance in many countries, and therefore exploiting the natural variation that exists in key crop characteristics represents an exciting and unexploited alternative.

Natural variation in photosynthetic capacity

Photosynthetic traits have been recognised previously as a potential source of natural variation that could be exploited for incorporation into breeding programmes to increase yield (Lawson *et al.*, 2012; Driever *et al.*, 2014; Faralli *et al.*, 2019). Using standard IRGA techniques (i.e. A/C_i) allowed us to take photosynthetic measurements in 200 wheat genotypes from a germplasm that captures 80% of the single nucleotide polymorphism variation in North–West European bread wheat (Mackay *et al.*, 2014), providing the largest screen to date of several photosynthetic parameters of the flag leaf. We observed significant variation in both photosynthetic capacity (V_{cmax} , J_{max} and A_{max}) and light saturated rates of photosynthesis (A_{sat}), highlighting the extent of intra-specific diversity that exists within UK bread wheat. The strong correlation we detected between V_{cmax} and J_{max} supports observations reported by other (Wullschleger, 1993). Furthermore, a simulation analysis in rice suggested that genetic variation in both Rubisco-limited (V_{cmax}) and electron transport-limited (J_{max}) photosynthesis increased rice yields by 22–29% across distinct locations and years (Yin and Struick, 2017), potentially providing genetic targets for exploitation to improve wheat photosynthesis in a similar way.

Although questions have been raised regarding how closely linked photosynthetic rates per unit of leaf area are with yield (Driever, et al., 2014; Zanella et al., 2023), ultimately photosynthesis is the primary determinant of all plant metabolic processes and therefore inevitably associated with reproductive processes (Slafer and Araus, 2007) and yield (Long *et al.*, 2006; Parry et al., 2011). Furthermore, many studies have reported increases in photosynthetic CO₂ assimilation along with rises in yield when different C₃ crops were grown in free-air carbon dioxide enrichment (FACE) facilities (Ainsworth and Long, 2005). Similarly, significant positive associations have been observed for different breeding lines in the field

between CO₂ uptake and g_s with grain yield components (Carmo-silva *et al.*, 2017; Blum, 1990; Fischer *et al.*, 1981; 1998; Reynolds *et al.*, 2000). However, contrary to this, many studies that have reported considerable variation in photosynthesis, could not demonstrate that these differences translated into changes in yield (e.g. Driever *et al.*, 2014; Chytky *et al.*, 2011; Sadras *et al.*, 2012). These contradicting findings may at least partially be due to the method used for photosynthetic assessment (Driever *et al.* 2014). Indeed, in most of the studies focusing on exploiting natural variation, photosynthesis is measured as maximum capacity which does not represent photosynthetic rates achieved in the field (Lawson *et al.*, 2012). Although instantaneous measurements during the day and standardized for a specific leaf (Gaju *et al.* 2016) provide a 'real' measure of photosynthesis at a specific moment in time, they fail to account for differences in microclimates; diurnal intra-canopy variation; conditional effects prior to measurement or circadian influences, all of which influence the measurements taken (Lawson *et al.*, 2012; Driever, *et al.*, 2014; Faralli *et al.* 2019). Here, we also determined the light saturated rate of photosynthesis (A_{sat}) (from the A/C_i analysis) which could be achieved in the field with sufficient light and no diffusional constraints from stomata (Lawson & Morison, 2004) .

Significant associations were observed between A_{sat} and V_{cmax} / J_{max} , suggesting that measuring A_{sat} could provide an important step to further define potential methods for estimating maximum carboxylation capacity of Rubisco and maximum electron transport for RuBP regeneration in wheat. Such strategies could be extremely beneficial for exploring and exploiting natural variation in photosynthesis as this is currently limited by the lengthy process for A/C_i measurements. While significant advances have been made recently in remote high-throughput measurement of photosynthetic capacity through hyperspectral imaging (Meacham-Hensold *et al.*, 2020; Burnett *et al.*, 2021), further research is needed to enhance the predictive capabilities of these tools across various crops and environmental conditions.

Although there was strong correlation between A_{sat} and A_{max} the differential rankings emphasize the influence of other factors on photosynthesis, for example limitation by low g_s which could impose a diffusional constraint on A_{sat} that would be removed by the high [CO₂] used to measure A_{max} . A_{sat} is much likely to represent realised carbon assimilation in the field further emphasising that a high photosynthetic potential does not always translate to a higher realised A as dynamic conditions and the impact on physiological processes needs to be taken into consideration (see below).

The strong co-ordination between J_{max} and V_{cmax} both within and between species that has been demonstrated here and in other studies (Wullschlegler, 1993), including those in which

photosynthesis has been manipulated (Harrison *et al.*, 2001), suggests that plants employ a conservative strategy (Wullschlegel, 1993). It has been suggested that this is to reduce the possibility of photoinhibition when carboxylation is limited, however this could also limit maximum photosynthetic rate under low light intensity (Walker *et al.*, 2014). In our work, the lack of any relationship between V_{cmax} and J_{max} with stomatal anatomy and/or rapidity suggests that operational g_s may limit photosynthetic carbon gain in wheat, corroborating the hypothesis in which speedy stomata may be a preferable trait for maintaining or increasing carbon fixation under natural environment (Lawson and Blatt, 2014).

Natural variation in dynamic stomatal responses

In order to function efficiently, CO₂ uptake for photosynthesis must be balanced with water loss from the plant, to ensure sufficient substrate for photosynthesis, without compromise to plant water status. Under steady state conditions there is usually a strong correlation between g_s and A (Wong *et al.*, 1977), however under dynamic conditions as experienced in the field, the slow stomatal response times to changing environmental conditions such as dynamic light patterns lead to a disconnect between g_s and A (Lawson & Vialet-Chabrand, 2018). The relative slower change in stomata compared with changes in photosynthetic rate can lead to diffusion constraints limiting rates of carbon assimilation (McAusland *et al.*, 2016; Lawson and Blatt, 2014; Vialet-Chabrand, *et al.*, 2017; Lawson & Vialet-Chabrand, 2018). Therefore, the kinetics of g_s responses to changing in light intensity such as changes in light intensity has been identified as a potential novel trait to increase photosynthesis (Long *et al.*, 2022) and plant water use efficiency (Lawson *et al.*, 2010; Lawson & Blatt, 2014; Matthews *et al.*, 2017). Previous work on natural variation for dynamic stomatal responses in wheat has been limited by the throughput, and therefore has been restricted to the evaluation of only a handful of genotypes. This is because such measurements usually rely on the use of IRGAs to measure stomatal responses during a step change in irradiance (e.g. McAusland *et al.*, 2016) which limits the throughput of this approach. Here, we used a novel thermal screening method to examine stomatal kinetics in 200 wheat genotypes. Leaf temperature is ultimately determined by stomatal conductance (as well as boundary layer and other physical features) and therefore thermography can be used to determine differences in g_s (Jones *et al.*, 2009) and has been successfully employed as a screen for identifying stomatal mutants (Wang *et al.*, 2004). It has also been proven to provide a rapid screen for g_s kinetics in response to changing irradiance (Vialet-Chabrand & Lawson 2019; 2020; Kimura *et al.*, 2020; Yamori *et al.*, 2020), although this requires a range of reference for energy balance calculations (see Vialet-Chabrand & Lawson 2019).

However, in order to use thermography to evaluate changes in g_s between different plant specimens and/or under changing conditions (temperature references (e.g. wet and dry reference) need to be included and maintained throughout the imaging process (see, Vialet-Chabrand & Lawson 2019; 2020). Additionally, knowledge of the boundary layer conductance and considerable computation power are required. Here we used a simplified approach that employed the use of only dry reference (Leinonen *et al.* 2006) along with controlled environmental chamber (similar to the one described by McAusland *et al.*, 2013 but modified for use in grasses) that controlled and maintained conditions around the leaves for image capture. The use of the chamber creating a constant boundary layer (see supplementary Dataset S1 for the calculation of boundary layer) simplified the calculation of g_s from thermal signatures. To validate the use of thermal images to determine the rapidity of g_s responses (K_i) to a step increase in light, we demonstrated a strong and significant positive correlation between K_i using by both methods and no significant differences between individual genotypes were observed using the two methods. However, a greater variation in K_i from IRGA measurements was evident, suggesting that K_i from thermography may if anything underestimate K_i . This is most likely explained by the fact that thermal images take account of the spatial and temporal variation across the leaf surfaces that is not required with the smaller chambers of IRGAs, and therefore possibly provide a more realistic representation of whole-leaf responses.

As with the photosynthetic parameters we demonstrated significant variation in both steady state g_s at $100 \mu\text{mol m}^{-2} \text{s}^{-1}$ PPFD, as well as the speed of g_s responses (K_i).

In general, natural variation was previously detected in these traits and this intraspecific variation was associated with stomatal anatomy both in wheat and barley (Faralli *et al.* 2019; Stevens *et al.* 2021) in a few genotypes. Although hypothesized and observed in studies focusing on interspecific diversity (e.g. Drake *et al.* 2013), in the present work, no link was found between stomatal anatomy and rapidity. Several anatomical, structural, and biochemical factors may affect stomatal rapidity to changing light and our data suggest that processes related to signalling, osmoregulation or solute transport play a greater role than anatomical features alone (Lawson and Vialet-Chabrand, 2018) for the variation observed. Significant associations were also observed between evaporative cooling and the magnitude of stomatal opening (δg_s) suggesting, not surprisingly, that the degree of stomatal opening is a key component for maintaining optimal leaf temperature under dynamic irradiance. Indeed, previous studies have associated steady-state maximum stomatal conductance with yield and canopy temperature depression under water-limiting and high temperature conditions (Fisher *et al.* 1986), suggesting that both stomatal dynamics and steady-state g_s represent a key target for maintaining optimal leaf temperature for photosynthesis. The fact that K_i and

δg_s were correlated with g_{smin} suggests that maintaining high basal g_s under low light could represent an important trait that primes a faster stomatal responsiveness to changes in light intensity. In the genetic material studied here g_{smin} and g_{smax} were positively associated and this may suggest that potential combination of preferable traits (e.g. inherently high g_{smax} , low K_i and high evaporative cooling) are present in wheat and that this can be exploited for additional fine-tuning of gas-exchange dynamics under fluctuating conditions. Wheat is amphistomatous and atypical, having greater stomatal numbers on the adaxial surface, although this is often correlated with the abaxial density, as shown here, which suggests a common signal that determines cell differentiation between the two surfaces. Furthermore, previous studies have shown that g_s is generally higher on the adaxial surface, which could have implications for gaseous diffusion and evaporative cooling for maintaining photosynthesis (Wall et al., 2022). This also highlights the potential of understanding the genetic targets that control stomatal development on the two surfaces to exploit for plants with enhanced diffusional capacity and/or cooling capacity and produce idiotypes for specific environments.

Interestingly, desirable stomatal traits were not necessarily observed in the same varieties as the desirable photosynthetic traits, suggesting that the presence of some traits may be at the expense of others. For example, the parental line Hereward had one of the fastest stomatal kinetic responses, but also one of the lowest A_{sat} and V_{cmax} values, whilst varieties such as Xi19 which had one of the highest photosynthetic capacities had one of the lowest K_i values. The rapid g_s responses in Hereward did not however result in a high δT , illustrating the importance of measuring actual g_s values and not just rapidity alone (Lawson & Blatt, 2014). However, as expected g_s could explain some of the photosynthetic responses observed. The parental line Robigous had low g_{smax} values, which most likely provides an explanation for the low A_{sat} observed, despite A_{max} being somewhere in the middle of the range. The low g_s values mostly likely created a diffusional constraint preventing high A_{sat} values to be achieved, which was overcome with the high CO_2 for the A_{max} measurements.

The dual imaging system used here for the kinetic responses incorporated chlorophyll fluorescence imaging of photosynthetic efficiency (Fq'/Fm') alongside thermography. Cultivar differences in Fq'/Fm' were apparent at the lower light intensities, reflecting the variation observed using IRGA measurements, however no significant differences at the high light intensity were found. This is most likely explained by the fact that firstly, Fq'/Fm' decreases with illumination and therefore the values are greatly reduced, hence limiting the potential variation range; and secondly in C3 species, that the end products of electron transport (ATP and NADPH) can also be utilized by sinks other than CO_2 assimilation (such as photorespiration) (Baker, 2008). For this reason, the measurements of Fq'/Fm' are unable to

distinguish differences in A that can be achieved through gas exchange, including those as a result of g_s diffusional constraints.

Conclusion

This is the first study providing evidence of wide variation for steady-state and dynamic gas-exchange traits in a bread wheat MAGIC population. This variation was detected using both standard eco-physiological approaches (IRGA) and novel methods (thermal imaging), allowing high throughput for stomatal dynamic phenotyping. Since natural variation in photosynthetic traits was identified in the wheat genotypes investigated, further work should focus on detecting the genetic loci controlling the traits employing larger numbers of RILs. Similarly, variation in dynamic stomatal responses was observed for the first time in the population as well as for g_{smax} , Δg_s and evaporative cooling using a novel method with higher throughput compared to standard techniques. This provides evidence of variability in bread wheat for dynamic g_s traits potentially providing unexploited targets for incorporation into ongoing breeding programmes. The strong relationships between our measured traits also provide proof of concept that taking the simpler measurement of A_{sat} and/or A_{max} could serve as a proxy for the more complex and time-consuming biochemical measurements of photosynthetic potential V_{cmax} and J_{max} . This is the first phenotyping study illustrating evidence of wide phenotypic variation in a wheat experimental population for several key-traits important in yield determination, thus stressing the possibility to further exploit this variation for detecting the genetic control of stomatal and photosynthetic characters for crop improvement.

Accepted Manuscript

Author Contributions:

MF, TL, JC KAC, and EO: designed the experiments; MF: performed all physiology experiments and data acquisition MF,SVC & GF carried out data analyses. SW collected stomatal data; MF and TL wrote the MS and all authors comment on the MS.

Conflicts of interest:

The authors have no conflicts to declare.

Funding

MF was supported via a BBSRC IPA funding with BASF (grant award to TL BB/N016831/1 and JC BB/N01698X/1). SW was funded by a (BBSRC) industrial studentship (1775930). BBSRC funding (BB/P027970/1) (BB/S005080/1) is also acknowledged.

Acknowledgements

We would like to thank Dr Phil Davey for technical assistance.

Raw data can be accessed from the Essex repository: Link will be provided once accepted.

Accepted Manuscript

References

- Ainsworth, E. A., & Long, S. P. (2005). What have we learned from 15 years of free-air CO₂ enrichment (FACE)? A meta-analytic review of the responses of photosynthesis, canopy properties and plant production to rising CO₂. *New phytologist*, 165(2), 351-372.
- Asseng, S., Guarin, J. R., Raman, M., Monje, O., Kiss, G., Despommier, D. D., ... & Gauthier, P. P. (2020). Wheat yield potential in controlled-environment vertical farms. *Proceedings of the National Academy of Sciences*, 117(32), 19131-19135.
- Baker, N. R. (2008). Chlorophyll fluorescence: a probe of photosynthesis in vivo. *Annu. Rev. Plant Biol.*, 59, 89-113.
- Billen, G., Aguilera, E., Einarsson, R., Garnier, J., Gingrich, S., Grizzetti, B., ... & Sanz-Cobena, A. (2024). Beyond the Farm to Fork Strategy: Methodology for designing a European agro-ecological future. *Science of The Total Environment*, 908, 168160.
- Blatt, M.R., (2000). Cellular signaling and volume control in stomatal movements in plants. *Annual review of cell and developmental biology*, 16(1), pp.221-241.
- Blum, A. (1990). Variation among wheat cultivars in the response of leaf gas exchange to light. *The Journal of Agricultural Science*. Cambridge University Press, 115(3), pp.305–311. DOI: 10.1017/S0021859600075717.
- Burnett, A.C., Anderson, J., Davidson, K.J., Ely, K.S., Lamour, J., Li, Q., Morrison, B.D., Yang, D., Rogers, A. and Serbin, S.P., (2021). A best-practice guide to predicting plant traits from leaf-level hyperspectral data using partial least squares regression. *Journal of Experimental Botany*, 72(18), pp.6175-6189.
- Carmo-Silva, E., Andralojc, P. J., Scales, J. C., Driever, S. M., Mead, A., Lawson, T., et al. (2017). Phenotyping of field-grown wheat in the UK highlights contribution of light response of photosynthesis and flag leaf longevity to grain yield. *Journal of Experimental Botany*. 68, 3473–3486. DOI: 10.1093/jxb/erx169
- Chytky, C., Hucl, P. and Gray, G. (2011). Leaf photosynthetic properties and biomass accumulation of selected western Canadian spring wheat cultivars. *Canadian Journal of Plant Science*, 91(2), pp.305-314. DOI:10.4141/CJPS09163.
- Drake, P. L., Froend, R. H., and Franks, P. J. (2013). Smaller, faster stomata: scaling of stomatal size, rate of response, and stomatal conductance. *Journal of Experimental Botany*. 64, 495–505. DOI: 10.1093/jxb/ers347

Driever, S. M., Lawson, T., Andralojc, P. J., Raines, C. A., and Parry, M. A. (2014). Natural variation in photosynthetic capacity, growth, and yield in 64 field-grown wheat genotypes. *Journal of Experimental Botany*, 65, 4959–4973. DOI: 10.1093/jxb/ eru253

Driever, S. M., Simkin, A. J., Alotaibi, S., Fisk, S. J., Madgwick, P. J., Sparks, C. A., *et al.* (2017). Increased SBPase activity improves photosynthesis and grain yield in wheat grown in greenhouse conditions. *Philosophical Transactions of the Royal Society B*, 372:20160384. DOI: 10.1098/rstb.2016.0384

Erenstein, O., Jaleta, M., Mottaleb, K. A., Sonder, K., Donovan, J., & Braun, H. J. (2022). Global trends in wheat production, consumption and trade. In *Wheat improvement: food security in a changing climate* (pp. 47-66). Cham: Springer International Publishing.

Evans, J. R. (2013). Improving photosynthesis. *Plant physiology*, 162(4), 1780-1793.

Faralli, M., Matthews, J., and Lawson, T. (2019). Exploiting natural variation and genetic manipulation of stomatal conductance for crop improvement. *Current Opinions in Plant Biology* 49, 1–7. DOI: 10.1016/j.pbi.2019. 01.003

Ferguson, J. N., McAusland, L., Smith, K. E., Price, A. H., Wilson, Z. A., & Murchie, E. H. (2020). Rapid temperature responses of photosystem II efficiency forecast genotypic variation in rice vegetative heat tolerance. *The Plant Journal*, 104(3), 839-855.

Fischer, R.A., Bidinger, F., Syme, J.R. and Wall, P.C. (1981). Leaf Photosynthesis, Leaf Permeability, Crop Growth, and Yield of Short Spring Wheat Genotypes Under Irrigation. *Crop Science*, 21(3), pp.367-373. DOI:10.2135/cropsci1981.0011183X002100030004x.

Fischer, R. A., & Stockman, Y. M. (1986). Increased kernel number in Norin 10-derived dwarf wheat: evaluation of the cause. *Functional Plant Biology*, 13(6), 767-784.

Fischer, R., Rees, D., Sayre, K., Lu, Z-M., Condon, A. and Saavedra, A.L. (1998). Wheat yield progress associated with higher stomatal conductance and photosynthetic rate, and cooler canopies. *Crop Science*, 38, pp.1467–1475. DOI: 10.2135/cropsci1998.0011183X003800060011x

Furbank, R. T., Sharwood, R., Estavillo, G. M., Silva-Perez, V., & Condon, A. G. (2020). Photons to food: genetic improvement of cereal crop photosynthesis. *Journal of Experimental Botany*, 71(7), 2226-2238. Harrison, E.P., Olcer, H., Lloyd, J.C., Long, S.P. and Raines, C.A., (2001). Cell and molecular biology, biochemistry and molecular physiology- small decreases in SBPase cause a linear decline in the apparent RuBP regeneration rate,

but do not affect Rubisco carboxylation. *Journal of Experimental Botany*, 52(362), pp.1779-1784. DOI: 10.1093/jexbot/52.362.1779

Hetherington, A. M., & Woodward, F. I. (2003). The role of stomata in sensing and driving environmental change. *Nature*, 424(6951), 901-908.

Jones, H. G., Serraj, R., Loveys, B. R., Xiong, L., Wheaton, A., & Price, A. H. (2009). Thermal infrared imaging of crop canopies for the remote diagnosis and quantification of plant responses to water stress in the field. *Functional Plant Biology*, 36(11), 978-989.

Kromdijk, J., Głowacka, K., Leonelli, L., Gabilly, S. T., Iwai, M., Niyogi, K. K., & Long, S. P. (2016). Improving photosynthesis and crop productivity by accelerating recovery from photoprotection. *Science*, 354(6314), 857-861.

Kimura, H., Hashimoto-Sugimoto, M., Iba, K., Terashima, I., Yamori, W. (2020) Improved stomatal opening enhances photosynthetic rate and biomass production in fluctuating light *J Exp Bot.* 6;71(7):2339-2350. DOI: 10.1093/jxb/eraa090

Lawson, T., Weyers, J., & A'Brook, R. (1998). The nature of heterogeneity in the stomatal behaviour of *Phaseolus vulgaris* L. primary leaves. *Journal of Experimental Botany*, 49(325), 1387-1395.

Lawson T., Oxborough K., Morison J.I.L. & Baker N.R. (2003) The response of guard cell photosynthesis to CO₂, O₂, light and water stress in a range of species are similar. *Journal Experimental Botany* 54 (388): 1743-1752. – DOI: 10.1093/jxb/erg186

Lawson T. & Morison J.I.L (2004) Stomatal Function and Physiology. In: *The Evolution of Plant Physiology; from whole plants to ecosystem*. Edited by Hemsley A.R. & Poole I. Elsevier Academic Press. 217-242.

Lawson T. (2009) Guard cell photosynthesis and stomatal function. *New Phytologist*. 181 (1): 13-34. – DOI: 10.1111/j.1469-8137.2008.02685.

Lawson, T., von Caemmerer, S., and Baroli, I. (2010). Photosynthesis and stomatal behaviour, in *Progress in Botany*, eds U. E. Luttge, W. Beyschlag, B. Budel, and D. Francis (*Berlin: Springer*), pp.265–304.

Lawson, T., and Blatt, M. R. (2014). Stomatal size, speed, and responsiveness impact on photosynthesis and water use efficiency. *Plant Physiology*. 164, 1556–1570. DOI: 10.1104/pp.114.237107

Lawson, T., Kramer, D. M., and Raines, C. A. (2012). Improving yield by exploiting mechanisms underlying natural variation of photosynthesis. *Current Opin. Biotechnol.* 23, 215–220. DOI: 10.1016/j.copbio.2011.12.012

Lawson, T., and Vialet-Chabrand, S. (2018). Speedy stomata, photosynthesis and plant water use efficiency. *New Phytologist.* 221, 93–98. DOI: 10.1111/nph.15330

Leinonen, I., Grant, O. M., Tagliavia, C. P. P., Chaves, M. M., & Jones, H. G. (2006). Estimating stomatal conductance with thermal imagery. *Plant, Cell & Environment*, 29(8), 1508-1518.

Long, S. P., Zhu, X. G., Naidu, S. L., and Ort, D. R. (2006). Can improvement in photosynthesis increase crop yields? *Plant Cell & Environment.* 29, pp.315–330. DOI: 10.1111/j.1365-3040.2005.01493.x

Long SP., Taylor SH., Burgess SJ., Carmo-Silva E., Lawson T., De Souza A., Leonelli L., Wang Y. (2022). Into the Shadows and Back into Sunlight: Photosynthesis in Fluctuating Light. *Annual Review of Plant Biology* 77: 617-648. doi: 10.1146/annurev-arplant-070221-024745.

Mackay, I. J., Bansept-Basler, P., Barber, T., Bentley, A. R., Cockram, J., Gosman, N., *et al.* (2014). An eight-parent multiparent advanced generation inter-cross population for winter-sown wheat: creation, properties, and validation. *Genes Genom. Genet.* 4, 1603–1610. DOI: 10.1534/g3.114.012963

Matthews J.A., Vialet-Chabrand, S.R., Lawson T. (2017) Diurnal variation in gas exchange: the balance between carbon fixation and water loss. *Plant Physiology* 174: 614-623. – DOI: 10.1104/pp.17.00152.

McAusland L., Davey P.A., Kanwal N., Baker N.R., Lawson T. (2013) A novel system for spatial and temporal imaging of intrinsic plant water use. *Journal of Experimental Botany.* 64 (16): 4993-5007. - DOI: 10.1093/jxb/ert288

McAusland L., Vialet-Chabrand S.R.M., Matthews J.S.A., Lawson T. (2015) Spatial and temporal responses in stomatal behaviour, photosynthesis and implications for water use efficiency. *Rhythm in plants: Dynamic responses in a dynamic environment.* Ed. Mancuso S., Shabala S. Springer. 97.

McAusland L., Vialet-Chabrand S., Davey P.A., Baker N.R., Brendel O., Lawson T. (2016) Effects of kinetics of light light-induced stomatal responses on photosynthesis and water-use efficiency. *New Phytologist.* 211 (4): 1209-1220. – DOI: 10.1111/nph.14000

- McAusland L., Violet-Chabrand S., Jauregui I., Burrige A., Hubbard-Edwards S., Pyke K., Fryer M., King I., King J., Edwards K., Carmo Silva E., Lawson T., Murchie E. (2020). Variation in key leaf photosynthesis traits across wheat wild relatives is accession-dependent not species-dependent. *New Phytologist*. 228: 1767-1780. Doi: /10.1111/nph.16832
- Meacham-Hensold, K., Fu, P., Wu, J., Serbin, S., Montes, C.M., Ainsworth, E., Guan, K., Dracup, E., Pederson, T., Driever, S. and Bernacchi, C. (2020). Plot-level rapid screening for photosynthetic parameters using proximal hyperspectral imaging. *Journal of Experimental Botany*, 71(7), pp.2312-2328. DOI: 10.1093/jxb/eraa068
- Murchie E.H. and Lawson T. (2013) Chlorophyll fluorescence analysis: a guide to good practice and understanding some new applications. *Journal of Experimental Botany*. 64 (13): 3983-3998. – DOI: 10.1093/jxb/ert208
- Parry, M. A., Reynolds, M., Salvucci, M. E., Raines, C., Andralojc, P. J., Zhu, X. G., ... & Furbank, R. T. (2011). Raising yield potential of wheat. II. Increasing photosynthetic capacity and efficiency. *Journal of experimental botany*, 62(2), 453-467.
- Outlaw, W. H. Jr. (2003). Integration of cellular and physiological functions of guard cells. *Crit. Rev. Plant Sci*. 22, 503–529. DOI: 10.1080/713608316
- Qu, M., Hamdani, S., Li, W., Wang, S., Tang, J., Chen, Z., *et al.* (2016). Rapid stomatal response to fluctuating light: an under-explored mechanism to improve drought tolerance in rice. *Funct. Plant Biol.* 43, 727–738. DOI: 10.1071/FP15348
- Raines, C. A. (2011). Increasing photosynthetic carbon assimilation in C3 plants to improve crop yield: current and future strategies. *Plant physiology*, 155(1), 36-42.
- Ray, D. K., West, P. C., Clark, M., Gerber, J. S., Prishchepov, A. V., & Chatterjee, S. (2019). Climate change has likely already affected global food production. *PloS one*, 14(5), e0217148.
- Reynolds, T.L. (2000). Effects of calcium on embryogenic induction and the accumulation of abscisic acid, and an early cysteine-labelled metallothionein gene in androgenic microspores of *Triticum aestivum*. *Plant Science*, 150(2), pp.201-207. DOI: 10.1016/S0168-9452(99)00187-9
- Sadras, V.O., Lawson, C. and Montoro, A., (2012) Photosynthetic traits in Australian wheat varieties released between 1958 and 2007. *Field Crops Research*, 134, pp.19-29. DOI: 10.1016/j.fcr.2012.04.012

Salter, W. T., Merchant, A. M., Richards, R. A., Trethowan, R., and Buckley, T. N. (2019). Rate of photosynthetic induction in fluctuating light varies widely among genotypes of wheat. *Journal of Experimental Botany*. DOI: 10.1093/jxb/erz100 [Epub ahead of print].

Sharkey, T. D., & Raschke, K. (1981). Separation and measurement of direct and indirect effects of light on stomata. *Plant physiology*, 68(1), 33-40.

Slafer, G.A., (2003) Genetic basis of yield as viewed from a crop physiologist's perspective. *Annals of Applied Biology*, 142(2), pp.117-128. DOI:10.1111/j.1744-7348.2003.tb00237.x

Slafer, G.A. and Araus, J.L., (2007) Physiological traits for improving wheat yield under a wide range of conditions. In: J.H.J. Spiertz, P.C. Struik, and H.H. van Laar, eds. *Scale and Complexity in Plant Systems Research: Gene-Plant-Crop Relations*. Volume 21. Dordrecht: Springer, pp.145-154.

South, P. F., Cavanagh, A. P., Liu, H. W., & Ort, D. R. (2019). Synthetic glycolate metabolism pathways stimulate crop growth and productivity in the field. *Science*, 363(6422), eaat9077.

Stevens J, Faralli M, Wall S, Stamford JD, Lawson T. (2021) Stomatal Responses to Climate Change. *Photosynthesis, Respiration and Climate change*. Springer. Edt. K. Becklin, J. Ward, D.A. Way. 7-47.

Talbott, L. D., Rahveh, E., & Zeiger, E. (2003). Relative humidity is a key factor in the acclimation of the stomatal response to CO₂. *Journal of Experimental Botany*, 54(390), 2141-2147.

Taylor, S. H., and Long, S. P. (2017). Slow induction of photosynthesis on shade to sun transitions in wheat may cost at least 21% of productivity. *Philosophical Transactions of the Royal Society B*, 372:20160543. DOI: 10.1098/rstb.2016.0543

Vialet-Chabrand, S., Dreyer, E., and Brendel, O. (2013). Performance of a new dynamic model for predicting diurnal time courses of stomatal conductance at the leaf level. *Plant Cell & Environment*. 3, 1529–1546. DOI: 10.1111/pce.12086

Vialet-Chabrand, S., and Lawson, T. (2019). Dynamic leaf energy balance: deriving stomatal conductance from thermal imaging in a dynamic environment. *Journal of Experimental Botany*. DOI: 10.1093/jxb/erz068.

Violet-Chabrand, S. R., Matthews, J. S., McAusland, L., Blatt, M. R., Griffiths, H., and Lawson, T. (2017). Temporal dynamics of stomatal behaviour: modelling and implications for photosynthesis and water use. *Plant Physiology*, 174, 603–613. DOI: 10.1104/pp.17.00125

Violet-Chabrand, S. and Lawson, T. (2020). Thermography methods to assess stomatal behaviour in a dynamic environment. *Journal of Experimental Botany*, 71, pp.2329–2338. DOI: 10.1093/jxb/erz573

Voss-Fels, K. P., Cooper, M., & Hayes, B. J. (2019). Accelerating crop genetic gains with genomic selection. *Theoretical and Applied Genetics*, 132, 669-686.

Walker, A. P., Beckerman, A. P., Gu, L., Kattge, J., Cernusak, L. A., Domingues, T. F., ... & Woodward, F. I. (2014). The relationship of leaf photosynthetic traits— V_{cmax} and J_{max} —to leaf nitrogen, leaf phosphorus, and specific leaf area: a meta-analysis and modeling study. *Ecology and evolution*, 4(16), 3218-3235.

Wang, Y., Holroyd, G., Hetherington, A. M., & Ng, C. K. Y. (2004). Seeing 'cool' and 'hot'—infrared thermography as a tool for non-invasive, high-throughput screening of Arabidopsis guard cell signalling mutants. *Journal of Experimental Botany*, 55(400), 1187-1193.

Wall, S., Cockram, J., Violet-Chabrand, S., Van Rie, J., Gallé, A. and Lawson, T., (2023). The impact of growth at elevated [CO₂] on stomatal anatomy and behavior differs between wheat species and cultivars. *Journal of Experimental Botany*. 74 (9), 2860-2874. DOI: 10.1093/jxb/erad011

Wall, S., Violet-Chabrand, S., Davey, P., Van Rie, J., Galle, A., Cockram, J., & Lawson, T. (2022). Stomata on the abaxial and adaxial leaf surfaces contribute differently to leaf gas exchange and photosynthesis in wheat. *New Phytologist*, 235(5), 1743–1756. DOI: 10.1111/nph.18257

Weyers JDB., Lawson T. (1997) Heterogeneity in stomatal characteristics. *Advances in Botanical Research*. 26: 317-352. DOI: 10.1016/S0065-2296(08)60124-X

Weyers JDB., Lawson T., Peng Z Y. (1997) Variation in stomatal characteristics at the whole-leaf level. SEB Seminar Series volume - Scaling Up. Edited by van Gardingen, P.R., Foody G.M., Curran, P.J., Cambridge University Press, Cambridge. 63: 129-149.

Wullschlegel, S.D. (1993). Biochemical limitations to carbon assimilation in C₃ plants—a retrospective analysis of the A/C_i curves from 109 species. *Journal of Experimental Botany*, 44(5), pp.907-920. DOI: 10.1093/jxb/44.5.907

Yamori, W., Kusumi, K., Iba, K. and Terashima, I., (2020). Increased stomatal conductance induces rapid changes to photosynthetic rate in response to naturally fluctuating light conditions in rice. *Plant, Cell & Environment*, 43(5), pp.1230-1240. DOI: 10.1111/pce.13725

Yoshiyama, Y., Wakabayashi, Y., Mercer, K.L., Kawabata, S., Kobayashi, T., Tabuchi, T. and Yamori, W., (2024). Natural genetic variation in dynamic photosynthesis is correlated with stomatal anatomical traits in diverse tomato species across geographical habitats. *Journal of Experimental Botany*. DOI.org/10.1093/jxb/erae082

Yin, X. and Struik, P.C., (2017) Can increased leaf photosynthesis be converted into higher crop mass production? A simulation study for rice using the crop model GECROS. *Journal of Experimental Botany*, 68(9), pp.2345-2360. DOI: 10.1093/jxb/erx085

Zanella, C. M., Rotondo, M., McCormick-Barnes, C., Mellers, G., Corsi, B., Berry, S., ... & Cockram, J. (2023). Longer epidermal cells underlie a quantitative source of variation in wheat flag leaf size. *New Phytologist*, 237(5), 1558-1573.

Zeiger, E., & Zhu, J. (1998). Role of zeaxanthin in blue light photoreception and the modulation of light-CO₂ interactions in guard cells. *Journal of Experimental Botany*, 433-442.

Zelitch, I. (1982). The close relationship between net photosynthesis and crop yield. *Bioscience* 32, 796–802. DOI: 10.2307/1308973

Zhang, Q., Peng, S., & Li, Y. (2019). Increase rate of light-induced stomatal conductance is related to stomatal size in the genus *Oryza*. *Journal of Experimental Botany*, 70(19), 5259-5269.

Accepted Manuscript

Figure legends

Figure 1. Comparison of methods for the measurement of stomatal opening. (A) Time constant for stomatal opening analysed via an infra-red gas analyser (dark grey) and the dual-imager (light grey) (n=3-7) in a sub-set of wheat genotypes. Data were analysed with two-way ANOVA and significant differences are indicated. (B) The linear association between the two methods. Data are means and fitting was carried out via linear regression.

Figure 2. Steady-state photosynthetic traits estimated via A/C_i curves. A) The variation between lines for photosynthetic CO_2 uptake at saturating light and ambient CO_2 concentration (A_{sat}). B) The variation between lines for photosynthetic CO_2 uptake at saturating light and elevated CO_2 concentration (A_{max}). For graphs, horizontal lines within boxes indicate the median and boxes indicate the upper (75%) and lower (25%) quartiles. Whiskers indicate the ranges of the minimum and maximum values. Circles indicate outliers. Data were analysed with ANCOVA (n=2-10) and p-values for the main effects are shown in the graph.

Figure 3. Biochemical traits estimated via A/C_i curves. (A) The variation between genotypes for the maximum velocity for Rubisco carboxylation (V_{cmax}). (B) The variation between genotypes for the maximum electron transport rate for RuBP regeneration (J_{max}). For graphs, horizontal lines within boxes indicate the median and boxes indicate the upper (75%) and lower (25%) quartiles. Whiskers indicate the ranges of the minimum and maximum values, and dots indicate outliers. Data were analysed with ANCOVA (n=2-10), p-values are indicated.

Figure 4. Maximum stomatal conductance under near-saturating light (g_{smax}), time for stomatal opening after a step change in light (K_i), evaporative cooling capacity (δT) and the difference between maximum stomatal conductance under near-saturating light and stomatal conductance before the step-change in light (δg_s) estimated with thermal imaging. For graphs, horizontal lines within boxes indicate the median and boxes indicate the upper (75%) and lower (25%) quartiles. Whiskers indicate the ranges of the minimum and maximum values. Data were analysed with ANCOVA (n=2-10) and p-values are shown in the graph

Figure 5. PSII operating efficiency at $100 \mu\text{mol m}^{-2} \text{s}^{-1}$ PPFD (F_q'/F_m' low light), PSII operating efficiency after 30 minutes at $1000 \mu\text{mol m}^{-2} \text{s}^{-1}$ PPFD (F_q'/F_m' high light) and non-photochemical quenching after 30 minutes at $1000 \mu\text{mol m}^{-2} \text{s}^{-1}$ PPFD (NPQ). Data were estimated via chlorophyll fluorescence imaging. For graphs, horizontal lines within boxes indicate the median and boxes indicate the upper (75%) and lower (25%) quartiles. Whiskers

indicate the ranges of the minimum and maximum values. Data were analysed with ANCOVA (n=2-10) and p-values are shown in the graph

Figure 6. Stomatal anatomical traits for a subset of the lines used for photosynthetic and dynamic screening. In A, the adaxial stomatal density (SD) is shown while in B) the abaxial SD is presented. For graphs, horizontal lines within boxes indicate the median and boxes indicate the upper (75%) and lower (25%) quartiles. Whiskers indicate the ranges of the minimum and maximum values. Data were analysed with one way-ANOVA (n=2-10) and p-values are shown in the graph

Figure 7. Multiple scatter plots for traits assessed in this work. In each panel, Pearson coefficient is shown for each correlation well as distribution. Significant associations are discussed in the text.

Accepted Manuscript

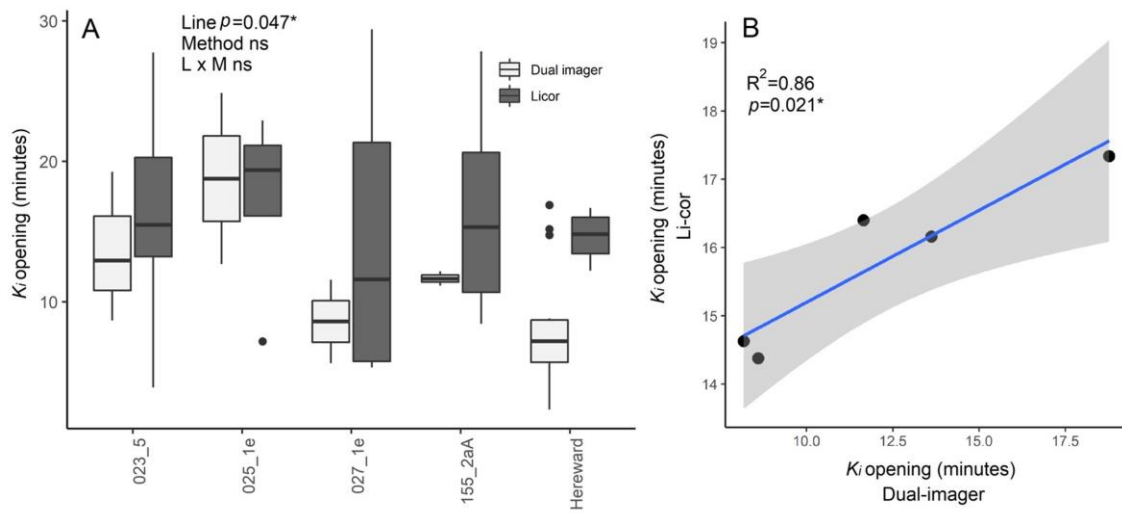


Figure 1. Comparison of methods for the measurement of stomatal opening. (A) Time constant for stomatal opening analysed via an infra-red gas analyser (dark grey) and the dual-imager (light grey) ($n=3-7$) in a sub-set of wheat genotypes. Data were analysed with two-way ANOVA and significant differences are indicated. (B) The linear association between the two methods. Data are means and fitting was carried out via linear regression.

Accepted Manuscript

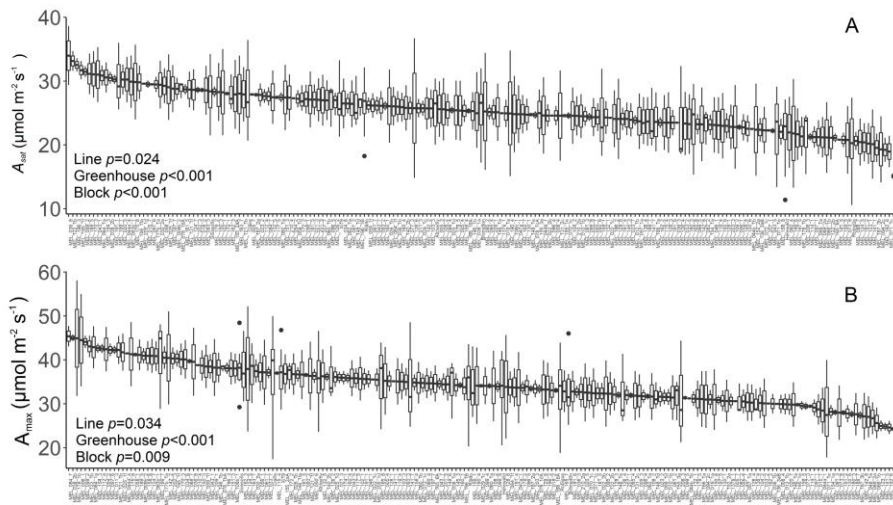


Figure 2. Steady-state photosynthetic traits estimated via A/C_i curves. A) A_{sat} The variation between lines for photosynthetic CO_2 uptake at saturating light and ambient CO_2 concentration (A_{sat}). B) A_{max} The variation between lines for photosynthetic CO_2 uptake at saturating light and elevated CO_2 concentration (A_{sat}). For graphs, horizontal lines within boxes indicate the median and boxes indicate the upper (75%) and lower (25%) quartiles. Whiskers indicate the ranges of the minimum and maximum values. Circles indicate outliers. Data were analysed with ANCOVA ($n=2-10$) and p -values for the main effects are shown in the graph.

Accepted Manuscript

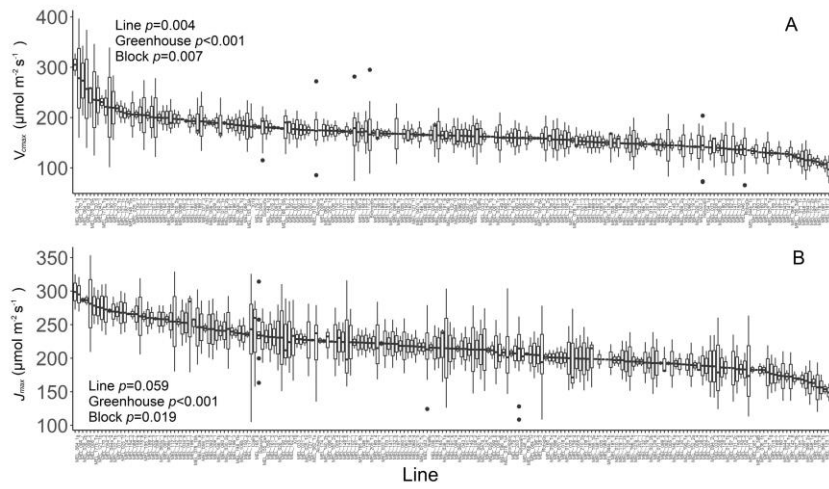


Figure 3. Biochemical traits estimated via A/C_i curves. (A) The variation between genotypes for the maximum velocity for Rubisco carboxylation (V_{cmax}). (B) The variation between genotypes for the maximum electron transport rate for RuBP regeneration (J_{max}). For graphs, horizontal lines within boxes indicate the median and boxes indicate the upper (75%) and lower (25%) quartiles. Whiskers indicate the ranges of the minimum and maximum values, and dots indicate outliers. Data were analysed with ANCOVA ($n=2-10$), p -values are indicated.

Accepted Manuscript

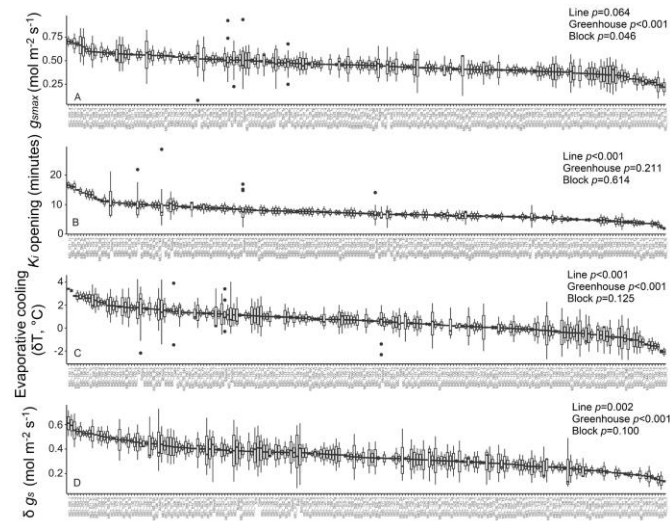


Figure 4. Maximum stomatal conductance under near-saturating light (g_{smax}), time for stomatal opening after a step change in light (K), evaporative cooling capacity (δT) and the difference between maximum stomatal conductance under near-saturating light and stomatal conductance before the step-change in light (δg_s) estimated with thermal imaging. For graphs, horizontal lines within boxes indicate the median and boxes indicate the upper (75%) and lower (25%) quartiles. Whiskers indicate the ranges of the minimum and maximum values. Data were analysed with ANCOVA ($n=2-10$) and p-values are shown in the graph

Accepted Manuscript

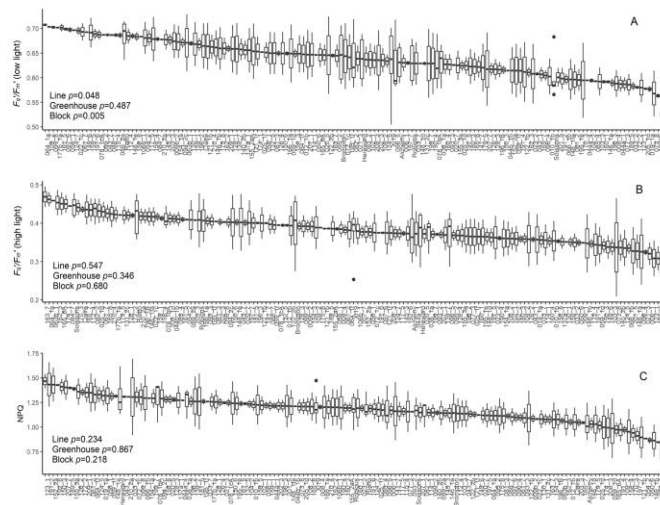


Figure 5. PSII operating efficiency at $100 \mu\text{mol m}^{-2} \text{s}^{-1}$ PPFD (F_q/F_m' low light), PSII operating efficiency after 30 minutes at $1000 \mu\text{mol m}^{-2} \text{s}^{-1}$ PPFD (F_q/F_m' high light) and non-photochemical quenching after 30 minutes at $1000 \mu\text{mol m}^{-2} \text{s}^{-1}$ PPFD (NPQ). Data were estimated via chlorophyll fluorescence imaging. For graphs, horizontal lines within boxes indicate the median and boxes indicate the upper (75%) and lower (25%) quartiles. Whiskers indicate the ranges of the minimum and maximum values. Data were analysed with ANCOVA ($n=2-10$) and p-values are shown in the graph

Accepted Manuscript

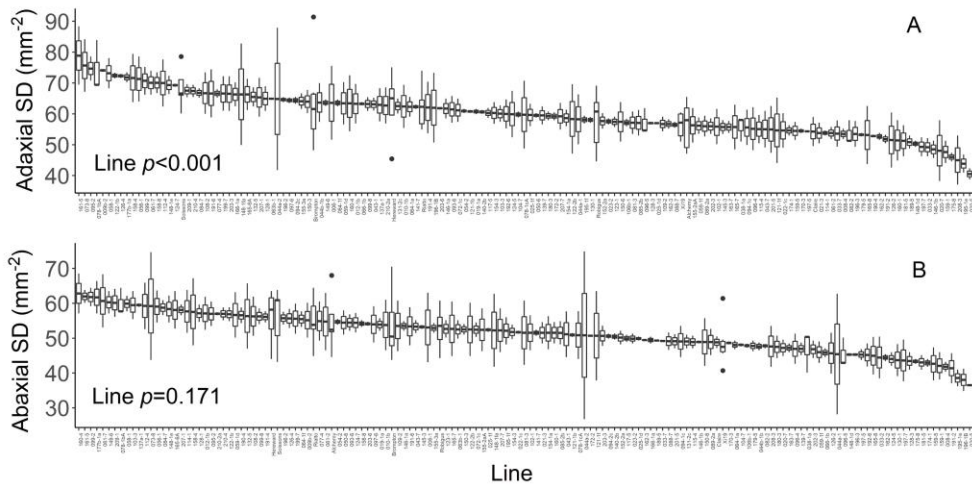


Figure 6. Stomatal anatomical traits for a subset of the lines used for photosynthetic and dynamic screening. In A, the adaxial stomatal density (SD) is shown while in B) the abaxial SD is presented. For graphs, horizontal lines within boxes indicate the median and boxes indicate the upper (75%) and lower (25%) quartiles. Whiskers indicate the ranges of the minimum and maximum values. Data were analysed with one way-ANOVA ($n=2-10$) and p-values are shown in the graph

Accepted Manuscript

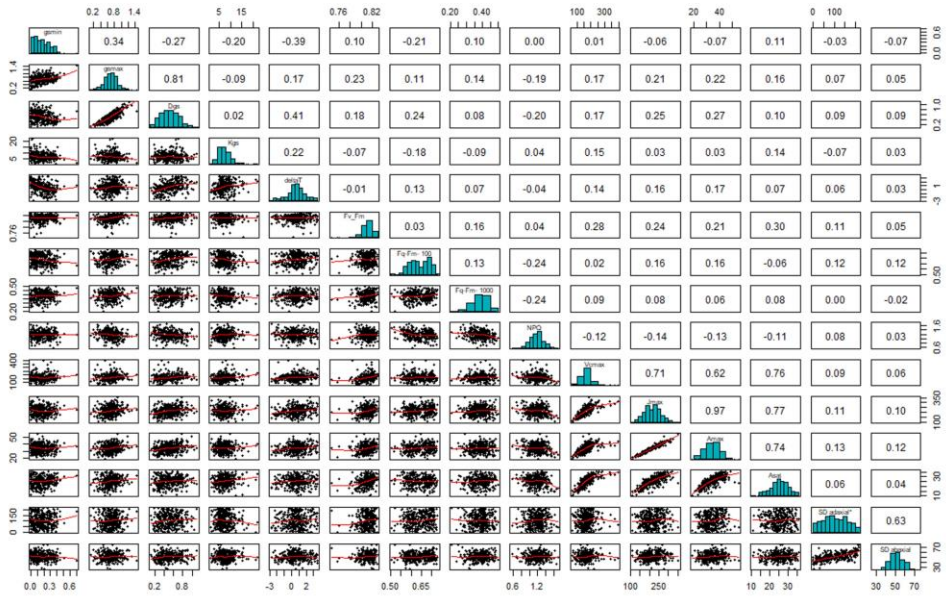


Figure 7. Multiple scatter plots for traits assessed in this work. In each panel, Pearson coefficient is shown for each correlation well as distribution. Significant associations are discussed in the text.

Accepted Manuscript